AFM and optical measurements on photonic-crystal slabs

Bachelor thesis
Rick Leijssen

Supervisors
Eduard Driessen
Michiel de Dood
Quantum Optics & Quantum Information,
Universiteit Leiden

August 27, 2009

Contents

1 Introduction **2**
- 1.1 Planar waveguides . . . 2
- 1.2 Periodic structures . . . 2
- 1.3 Manufacturing of the samples . . . 4
- 1.4 Spontaneous parametric downconversion . . . 4

2 AFM measurements on photonic crystal slabs **4**
- 2.1 Imaging the holes . . . 5
- 2.2 Measuring layer thicknesses . . . 6
- 2.3 Membrane buckling and stiffness . . . 6
  - 2.3.1 Height differences . . . 6
  - 2.3.2 Force curves . . . 9

3 Transferring membranes to gel **9**
- 3.1 Method . . . 10
- 3.2 Changing optical properties . . . 10
  - 3.2.1 Transmittivity of the gel . . . 10
  - 3.2.2 Change in photonic band structure . . . 13

4 Possible SPDC in photonic crystals **13**
- 4.1 Optical properties . . . 14
- 4.2 Luminescence of the GaAs substrate . . . 19
- 4.3 Possible observation of SPDC . . . 20
- 4.4 Power dependence of this signal . . . 22
- 4.5 Resonance shifting at high pump power . . . 23

5 Discussion **24**

6 Summary **25**

1 Introduction

In this thesis we study the properties of photonic-crystal slabs, using a variety of techniques including atomic force microscopy (AFM), spectroscopy, and direct imaging of resonances. In addition, we try to observe spontaneous parametric downconversion (SPDC) in the crystals, a nonlinear process where one photon produces two photons, whose energy adds up to the energy of the original photon.

Photonic crystals are structures with a periodic refractive index in one or more directions. In this thesis, we study photonic-crystal slabs, which are planar membranes patterned with a lattice of holes. The photonic-crystal slabs exhibit resonant modes where light can be coupled into or out of a waveguide mode in the slab[1, 2, 3, 4].

1.1 Planar waveguides

Waveguide modes can exist in planar structures which have a higher refractive index than the surrounding medium. The light is bound to the waveguide by total internal reflection from the interfaces, but is free to propagate in the plane of the structure. Two kinds of waveguide modes exist, namely those with the electric field perpendicular to the slab (Transverse Electric, or TE) and those with the electric field in the plane of the slab (Transverse Magnetic, or TM).

Figure 1 shows the dispersion diagram for a planar waveguide with $n = 3.4$ (typical for the AlGaAs membranes we use) and thickness d, surrounded by air. Here ω is the angular frequency and $k = 2\pi/\lambda$ is the wave vector of a plane wave, and $k_{\|}$ is the component of the wave vector parallel to the slab. The blue and red curves show the dispersion of the TE and TM waveguide modes, respectively. In the grey area, the light is no longer confined to the slab by total internal reflection. In the black area, no propagating modes exist at all.

1.2 Periodic structures

The holes in the photonic-crystal slab act as scattering centers for the waveguide modes. Because of the periodicity of the holes, the scattering from them can interfere constructively in certain directions, creating diffraction, and thus light can couple from the surrounding medium to the waveguide mode or vice versa.

This is most easily visualized by imposing the periodicity of the holes on the dispersion relation of the guided modes. Figure 2 shows the dispersion diagram of the first two waveguide modes from figure 1 with a one-dimensional periodicity with reciprocal lattice vector $G = 2\pi/a$, constructed by repeating the dispersion relation.

In figure 2, it can be noticed that different waveguide modes cross. At such crossings, interaction between the modes can induce an avoided crossing between the curves, leading to a more complicated dispersion relation[3].

Also, guided modes now show up above the light line (in the grey area). Where this happens, diffraction from the periodic structure allows light to couple from the waveguide mode to the surrounding air or vice versa.

The modes show up in the reflection and transmission spectra of the photonic-crystal slabs as asymmetric peaks, which are caused by interference between a direct and a resonant contribution. In the direct contribution, light is directly

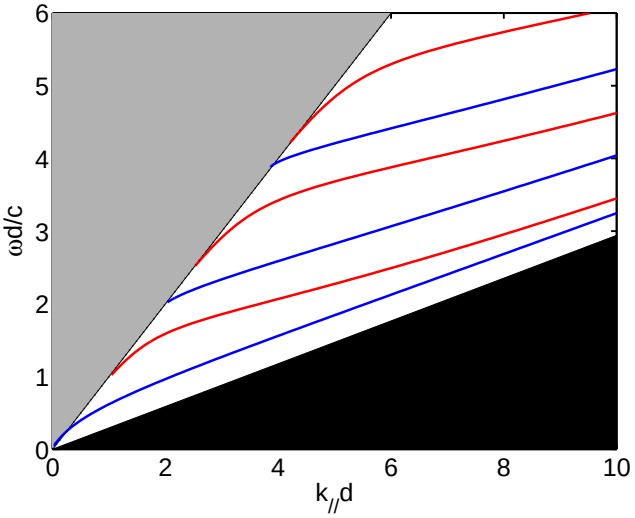

Figure 1: Dispersion diagram of a planar waveguide with $n = 3.4$ and thickness d, surrounded by air. The blue and red curves give the dispersion of the TE and TM waveguide modes, respectively. The grey area indicates the light cone, where light is not bound to the slab. The black area indicates the region where no propagating modes exist at all.

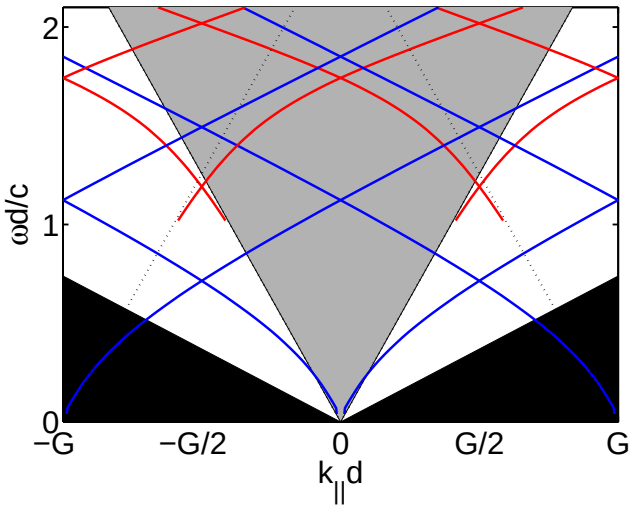

Figure 2: Construction of the dispersion relation of the first two modes of the waveguide of figure 1, that is patterned with a one-dimensional array of infinitesimal lines. The lattice period $a = 2.5d$, where d is the thickness of the slab. The grey area indicates the light cone. The dotted lines indicate diffraction orders into the surrounding air.

reflected or transmitted, without coupling to the waveguide modes, while in the resonant contribution, light is coupled into the modes of the structure and then diffracted back[5].

1.3 Manufacturing of the samples

Before the fabrication process, the wafers have the following composition:

SiN_x	150 nm	Etch mask
GaAs	100 nm	Protective capping layer
$Al_{0.35}Ga_{0.65}As$	150 nm	Photonic crystal layer
$Al_{0.7}Ga_{0.3}As$	1000 nm	Sacrificial layer
GaAs	$\sim$ 200 µm	Wafer

During the manufacturing process, a resist layer is added, which is then selectively exposed using an electron-beam writer to produce the hole lattice. This pattern is then etched into the layers below. After this, the SiN_x and GaAs are removed. Finally, the sacrificial layer is etched away beneath the holes. This produces a free-standing photonic-crystal membrane[6].

Sometimes the membranes can fall down and stick to the substrate (a 'touched down' membrane), because of problems in the manufacturing process or due to mechanical causes later on.

The membranes we used in this thesis all had a square lattice, except for a few samples we used for AFM measurements that had a hexagonal lattice. The membranes all had round holes. The membranes are characterized by the hole radius r and the distance between the holes, or lattice constant, a.

1.4 Spontaneous parametric downconversion

Spontaneous parametric downconversion (SPDC) is a non-linear optical process in a crystal, in which one photon with frequency ω_p is absorbed, and two photons at frequencies ω_a and $\omega_b = \omega_p - \omega_a$ are created. If there is also incident light at frequency ω_a, the output of ω_b and ω_a is amplified. This process is known as 'difference frequency generation' or 'parametric downconversion' (PDC)[7].

Nonlinear processes such as SPDC can only occur in materials which have a nonzero non-linear susceptibility $\chi^{(2)}$. GaAs and AlGaAs have this property. However, in bulk materials, nonlinear processes are not efficient, due to a phase mismatch (different phase velocity) of the pump wave and the generated waves. After one coherence length, the pump and downconverted waves are out of phase, and the newly-generated downconverted wave will interfere destructively with the previously generated wave. In our case however, the coherence length is of the same order of magnitude ($\sim$ 10 µm) as the decay length of the waveguide mode. Therefore, we can ignore phase matching considerations.

2 AFM measurements on photonic crystal slabs

Atomic Force Microscopy (AFM) is a widely-used form of scanning probe microscopy, where a cantilever with a sharp tip is scanned across the surface which is to be imaged. The deflection of the cantilever is used in a feedback loop with

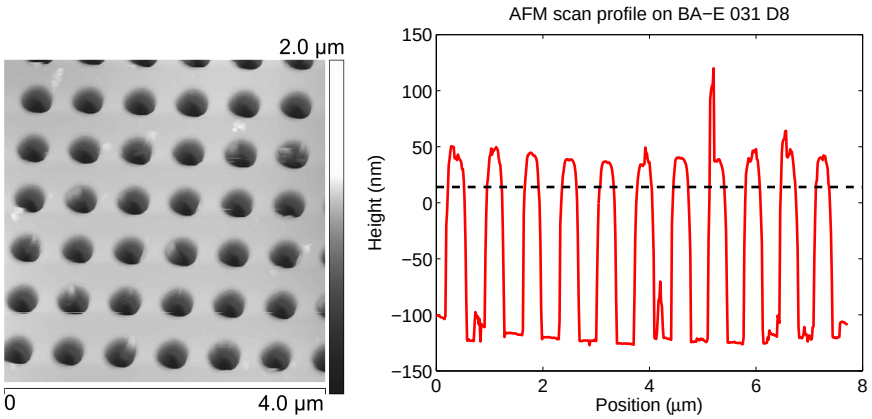

(a) AFM image of sample BA-E 031, cell C6. The photonic-crystal slab has $r = \sim 200$ nm and $a = 640$ nm.

(b) AFM cross section on sample BA-E 031, cell D8. This photonic-crystal slab has a hexagonal lattice with $r = \sim 200$ nm and $a = 640$ nm.

Figure 3: Typical AFM results.

a piëzo scanner to keep the tip at a constant height from the surface. In this way very small features can be resolved[8].

We used AFM to measure the topography of photonic-crystal slabs, on length scales from the size of the individual holes (~ 200 nm) up to the scale of folds in the membranes (~ 60 µm).

Compared to scanning electron microscopy (SEM), AFM offers the advantage of measuring height data, which gives information about the actual layer thicknesses on the sample.

We also used the AFM in force mode. In this mode, the cantilever is ramped up and down in one position and the deflection of the cantilever is measured. The obtained force-distance data was used to probe the (local) mechanical properties of the membrane.

2.1 Imaging the holes

On the scale of the individual holes, collections of holes can be imaged to gain information about the variation in hole radius r and the distance between the holes a. A typical AFM image is shown in figure 3. Figure 3a shows a two-dimensional height profile. Figure 3b shows a cross-section of the AFM data through the holes, of a membrane that is touched-down on the substrate.

To determine the hole radius r, we set a threshold height (indicated with the dashed line in figure 3b). All points lower than this height were considered to be part of the holes. We determined the area A of each individual hole, and assumed a circular shape of each hole, such that $r = \sqrt{A/\pi}$. The lattice constant a was determined by measuring the distance between the 'centers of mass' of the blobs.

The absolute values of the measured r and a depend on the calibration of the AFM scanner. The measured samples typically have $a = 640$ nm and

r = 200 nm; one of the piëzo scanners yielded values on one of the samples which were 15 % lower than specified. Another scanner exhibited a direction dependence of up to 4 % in its calibration, especially when operating the piëzo scanner in other directions than the default one.

This shows that the distance between the holes could actually be used to calibrate the scanners. Since the measured value of a doesn't rely on where the threshold value for the edge of the holes is taken, this calibration only depends on how well the manufacturing process is calibrated.

The value of r/a, the size of the holes *relative* to the distance between them, is independent of the calibration of the AFM scanner. This value does depend on taking an appropriate threshold value to define the edge of the holes, which introduces an error of about 5 %.

The statistical data on the thresholded images can also be used to calculate the standard deviations in r and a. These variations are about 2–4 % (3–6 nm) variation in r and 1–2 % (5–10 nm) variation in a. Both are within the resolution of the e-beam process used to manufacture these samples, which has a 10 nm beam step size and $\sim$ 10 nm resolution of the resist layer.

Note also that for a typical image with a size of 4 µm, each pixel has a size of 7.8 nm, which means the measured variations are already smaller than the pixel size. This scan range has been chosen to have a reasonable number of holes in the image, in order to be able to average out small defects.

2.2 Measuring layer thicknesses

The height information in the AFM images can be used to determine the thickness of the different layers in the sample. Figure 3b shows a cross section of an AFM image on a touched-down membrane. From a depth histogram of an entire AFM image on a touched-down membrane we find the thickness to be 162 $\pm$ 10 nm. This value is consistent with the design specification of $\sim$ 150 nm.

By scanning the edge of the membrane, the thickness of the GaAs capping layer, which is still present on the unpatterned substrate but is etched away on the membrane, can similarly be measured to be about 100 $\pm$ 10 nm thick.

Figure 4 shows an AFM image of a membrane with a larger lattice constant (a = 960 nm). In the image, an extra square structure is visible around each hole. The thickness of this structure is 100 $\pm$ 10 nm. This supports the hypothesis that this was a residue of the GaAs capping layer, which was not entirely removed during the manufacturing of the sample. Note that the existence of this extra GaAs layer can also be observed in the optical microscope, as a dark green color of the membrane.

2.3 Membrane buckling and stiffness

2.3.1 Height differences

The membranes are typically buckled up on the substrate. This is due to a small mismatch of the lattice constants of the $Al_{0.35}Ga_{0.65}As$ (l = 0.565603 nm[9] membrane layer and the GaAs (l = 0.565325) substrate, causing a small compressive strain in the membrane layer, that is released when the sacrificial layer is etched. The lattice mismatch is about 0.05 %, which would suggest a

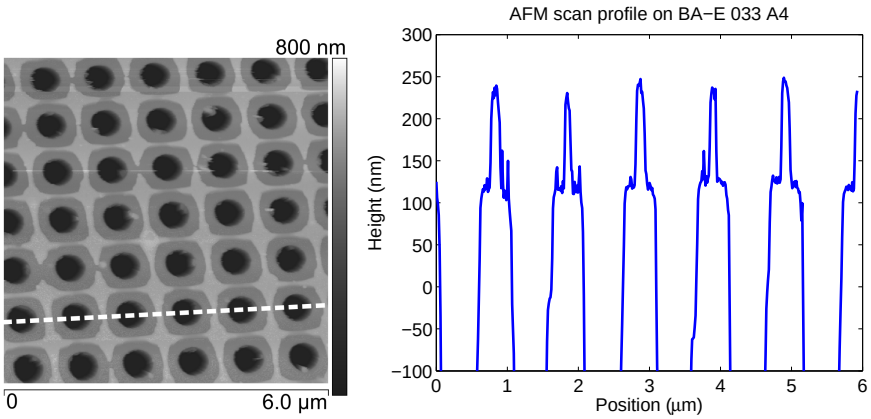

(a) AFM scan on sample BA-E 033, cell A4. The white dashed line indicates where the cross section in figure (b) is taken.

(b) AFM cross section along the white dashed line in figure (a). The extra GaAs top layer is clearly visible and can be seen to be about 100 nm thick.

Figure 4: AFM scan of sample BA-E 033, cell A4. Note the residue of the GaAs capping layer, which is about 100 nm thick.

height difference of $\sim$ 5 µm over a distance of 150 µm(with a typical slope of 1.9°).

An example of this buckling can be seen in the microscope image in figure 5, which was taken with an interference objective using green light at a wavelength of 549 nm. Each fringe thus corresponds to a height difference of 274.5 nm.

The white dashed arrow indicates a path from the edge of the membrane to the middle, and highest, point on the membrane. About 40 interference fringes can be counted along this line, which corresponds to a height difference of $\sim$ 10 µm. The membrane is about 300 µm wide, yielding a typical slope of 10 µm over 150 µm distance (3.8°).

The difference between the estimate based on the lattice mismatch and this measurement might be explained by the fact that the estimate was made in a 1-dimensional analysis, while the membrane is attached to the substrate at all of its edges. This 2-dimensional geometry causes additional stress, especially in the corners, which might cause the membrane to buckle up even more.

The buckling of the membranes can also be characterized using AFM. By scanning a large area, in this case 60x60 µm, the height difference across one of the folds can be measured. From figure 6b the height difference can be seen to be about 3 µm over 60 µm distance. Figure 6a can be used to check that the height is indeed decreasing monotonically.

However, during the scanning, the tip of the AFM was pushing the fold along, which could be seen in the optical microscope in the AFM setup. This means the actual slope of the membrane is higher than figure 6 indicates. The horizontal 'steps' in the AFM image were caused by the fold jumping to another position (the AFM image was made by scanning the horizontal lines one by one). In figure 6c it can even be seen that part of the fold has permanently changed position after the scan.

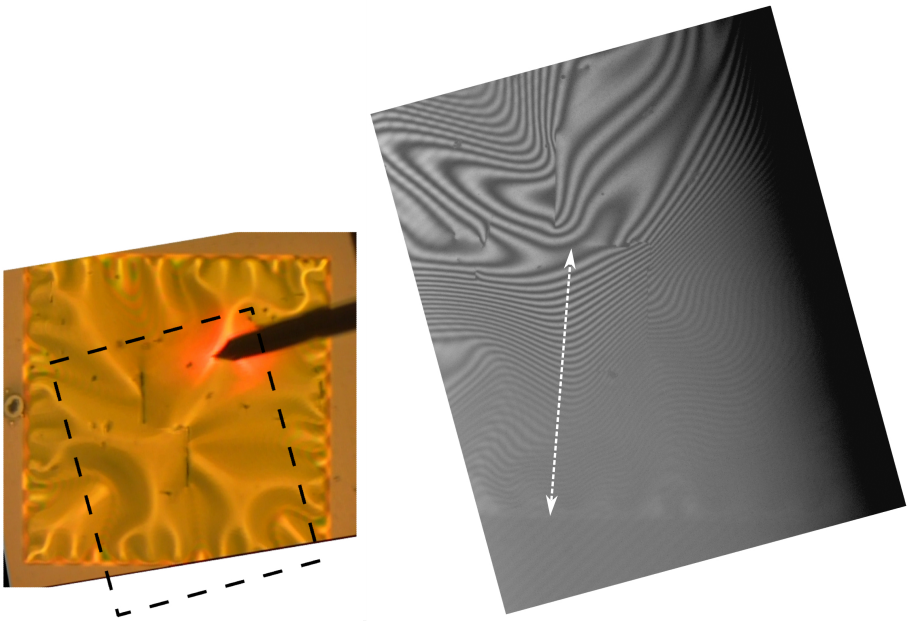

(a) Microscope image of the membrane in the AFM. The dashed lines indicate the field of view of the interference image in (b).

(b) Interference microscope image. The white dashed arrow indicates the path from the edge to the center of the membrane; about 40 fringes can be counted along this line. Each fringe corresponds to a height difference of 274.5 nm.

Figure 5: Interference microscope image of BA-E 033 A2.

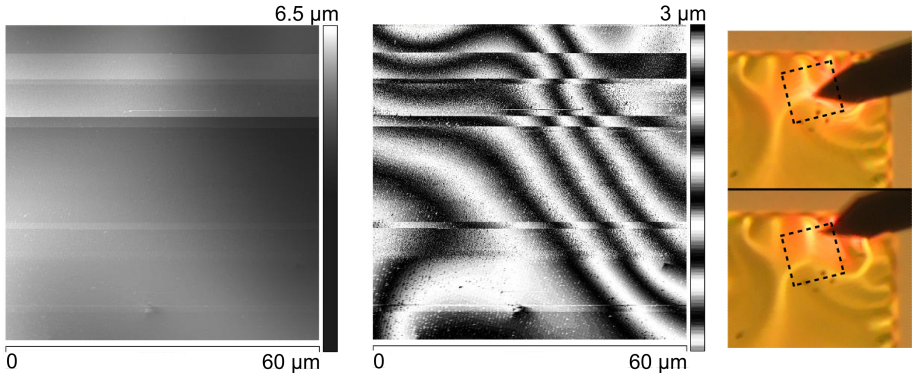

(a) AFM image with normal colorscale.

(b) The same AFM image with alternating colorscale. Each color band corresponds to 550 nm height difference.

(c) Optical microscope image.

Figure 6: AFM scan on sample BA-E 033, cell A2. In the optical microscope image in figure (c), the field of view of the AFM images is indicated. Also visible in figure (c) is that the fold in this scan range has moved to a new position after the scan.

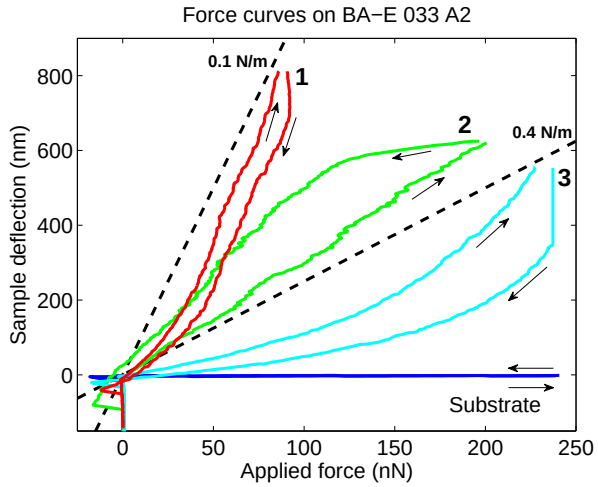

(a) Force curves at 3 different positions on sample BA-E 033, cell A2. The positions are indicated in figure (b). The black dashed lines are lines with spring constants 0.1 N/m and 0.4 N/m.

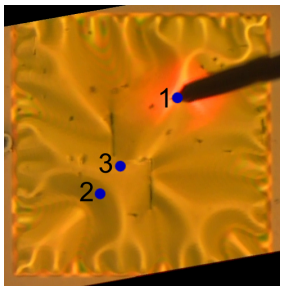

(b) Microscope image showing the positions where the force curves of figure 7a were taken.

Figure 7: Force curves on sample BA-E 033, cell A2 as free-standing membrane.

2.3.2 Force curves

The (local) stiffness of the membrane can be measured using the force curve mode of the AFM. In this mode the cantilever is ramped up and down at one position, while the deflection of the cantilever is recorded. The response of the membrane as a function of the exerted force can then be calculated sing the known spring constant of the cantilever (2 N/m).

Figure 7a shows the response of the membrane at a few different positions. As can be seen from this figure, the response is very position dependent. Measurements at the same position (not shown) are reproducible.

The 'down' and 'up' parts of the curves are different, and there is a small jump between them. This can be explained by the fact the membrane jumped into another position at the lowest point reached by the cantilever, which was also observed by watching the optical microscope during the measurement.

A very crude approximation of the effective spring constant of the membrane is made by taking the slope of the line from 0 to the end of the curve. This yields values of about 0.1 N/m (position 1) to 0.4 N/m (position 3). The lines corresponding to springs with these spring constants are plotted as black dashed lines in figure 7a. A spring constant of 0.1 N/m is comparable to a commercial silicon cantilever of 200 nm thickness, 40 µm length and 16 µm width[10].

3 Transferring membranes to gel

Membranes can be transferred from the GaAs substrate to a layer of gel on a glass substrate by simply sticking the samples to the gel and removing the substrate. This eliminates any luminescence from the GaAs substrate, and opens

the possibility of doing transmission measurements, since the gel and glass are both transparent.

For the gel, we use "Gel-Film", a Gel-Pak product which consists of a layer of transparent gel that is meant to immobilize devices to protect them during storage and/or transport. We used the gel with retention level 'X4'. The gel is transparent and can maintain its integrity up to 220 °C[11].

3.1 Method

To transfer the membranes to the gel, we take a piece of Gel-Film and place it on a microscope slide. On top of that we gently place the sample, membranes facing down, and remove it again. The membranes are then stuck to the gel and free from the substrate.

In figure 8, a typical membrane is shown both before and after the transfer. After the transfer the membrane is very flat and only has a few cracks. The interference microscope image in figure 8c confirms the flatness of the membrane (compare to figure 5 which is of a membrane still on the substrate). Figure 8d shows that the curvature which can be seen in the membrane is also present in the gel.

In figure 9 a membrane is shown which was imperfectly transferred: there are a few big folds which are 5–10 µm high, according to the amount of fringes that can be counted on them in the interference microscope image.

Figure 10 shows the sample BA-E 033, cell B4, which was used for optical measurements. The images on the gel were taken after the sample was damaged by focussing a high-powered laser on the membrane. This damaged one part of the cell significantly, but the other parts of the membrane are still usable.

We transferred about 20 membranes to gel, of which only about 5 had significant damage or folds from the transfer process. These were also the cases where the transfer was done the least carefully, so these problems can largely be avoided by taking more care during the transfer process.

3.2 Changing optical properties

3.2.1 Transmittivity of the gel

Before addressing the transmission of the photonic crystals, we first discuss the optical properties of the gel.

For transmission measurements, we used a normal-incidence setup. A Xenon lamp was used to illuminate the sample and the transmitted light was collected and sent into a fiber spectrometer.

Figure 11 shows the transmission spectrum of a layer of gel on a glass microscope slide. The measurements are normalized to transmission through air. It can be seen that the transmission is high (85–95 %) and reasonably flat.

The fact that the transmission through glass and gel in the infrared region is higher than the transmission through glass alone could be attributed to slow fluctuations in either detection efficiency of the detector or power output of the Xenon lamp. This would also explain the mismatch of the measurements where the 2 detection ranges overlap.

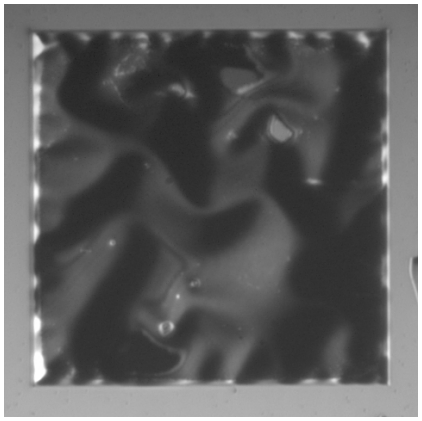

(a) Before transfer (on the substrate).

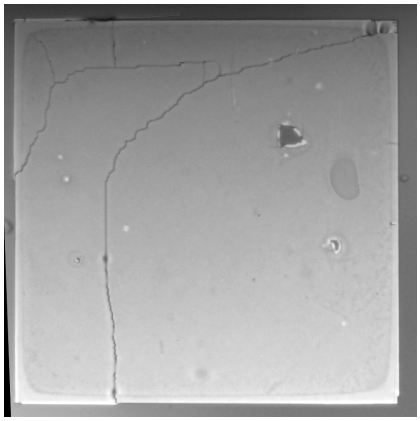

(b) After transfer to the gel.

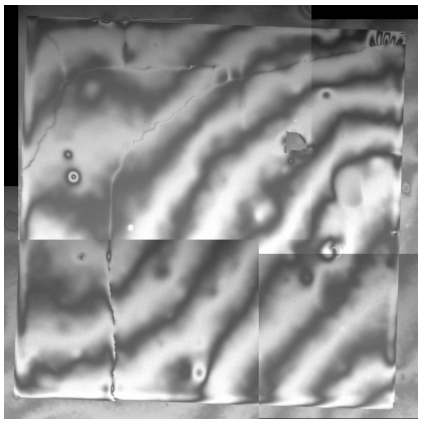

(c) Interference microscope image after transfer to the gel.

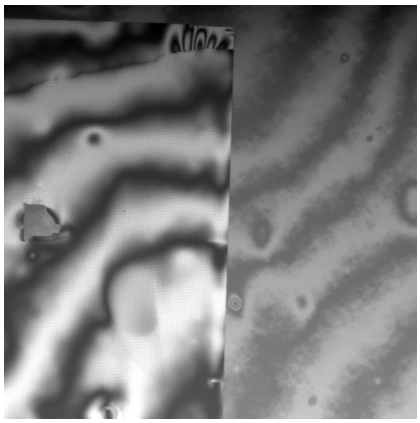

(d) Interference microscope image including gel.

Figure 8: Microscope images of sample BA-E 033, cell C4, before and after transfer to the gel.

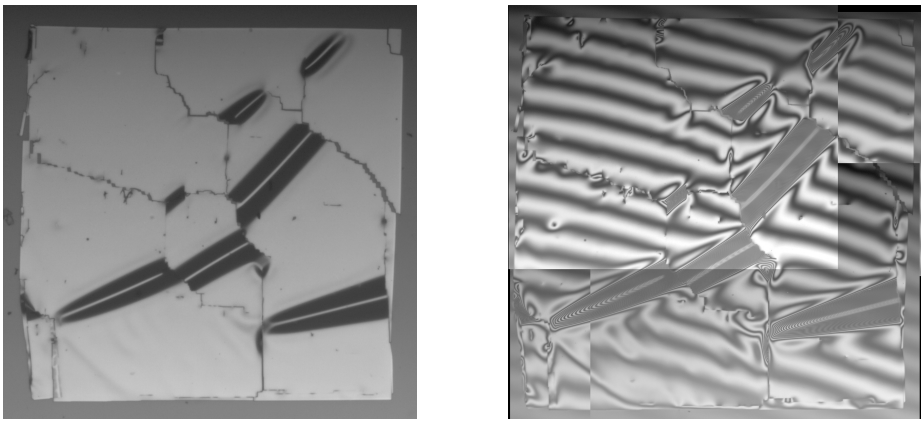

(a) After transfer to the gel.

(b) Interference microscope image after transfer to the gel

Figure 9: Microscope images of the imperfectly transferred sample BA-E 033, cell A2, after transfer to the gel.

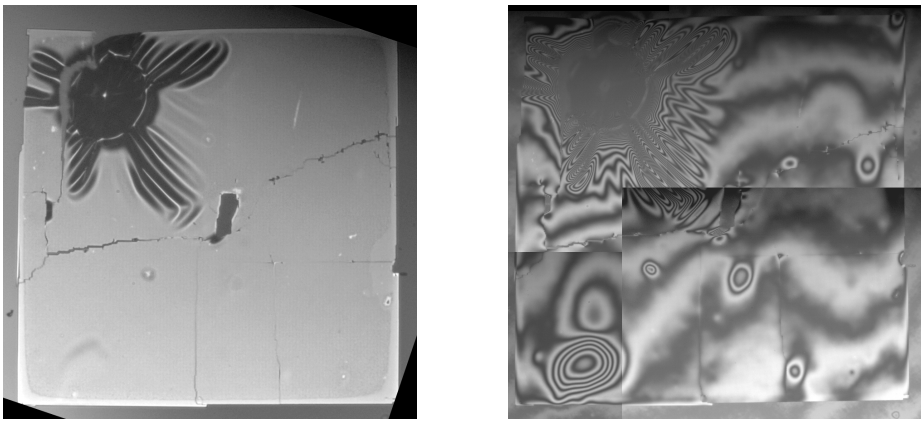

(a) After transfer to the gel.

(b) Interference microscope image after transfer to the gel.

Figure 10: Microscope images of sample BA-E 033, cell B4, which was used for optical measurements, after transfer to the gel. One part of the membrane was badly damaged by focussing a high-powered laser onto it, but the rest of the membrane is still usable.

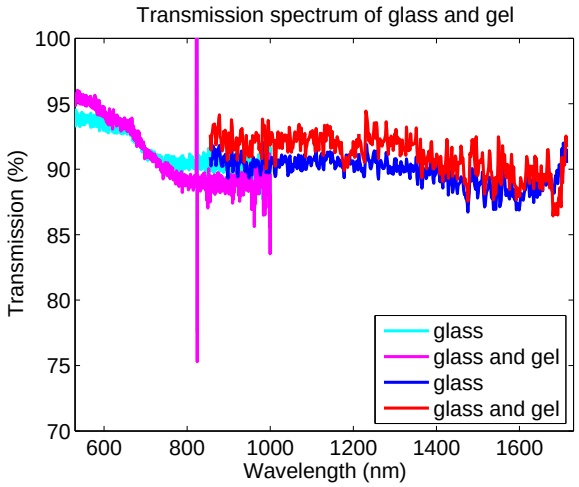

Figure 11: Transmission of a layer of gel on a glass microscope slide, at normal incidence. The spectra are normalized to transmission through air.

3.2.2 Change in photonic band structure

Figure 12 shows reflection and transmission spectra at normal incidence of a sample before and after transfer to the gel. In both curves, 2 sharp asymmetric peaks respectively dips are visible. These optical resonances are caused by the periodic structuring of the membrane. Note that the reflection and transmission are complementary, which means the peaks in reflectivity correspond to the dips in transmission and vice versa.

The resonances after transfer are shifted to the red compared to the resonances before transfer to gel. By measuring the position of the large peaks and dips in the 2 lines, the shift in the resonances due to the transfer to the gel was determined to be 12.5 nm to the red.

This redshift can be understood qualitatively using a simple waveguide model. Because the gel has a higher refractive index than air, the photonic band structure of the membranes changes. By introducing the gel on one side of the slab, the slope of the lightline (boundary of the grey area in figure 1) decreases, which will shift the waveguide modes down with it, towards the red.

4 Possible SPDC in photonic crystals

In order to try to observe spontaneous parametric downconversion (SPDC) in our photonic-crystal slabs, we used a setup to image the light from the membrane directly, because this setup has a higher NA and the CCD camera has a higher sensitivity than the spectrometer previously used to measure the resonances of the crystal.

We used the setup of [6], modified for transmission measurements. Figure 13 shows a schematic overview of this setup. Light from a tunable picosecond Ti:Sapphire laser is attenuated using a half-wave plate (HWF) and polarizer (P), by turning the half-wave plate in order to cross the output polarization of

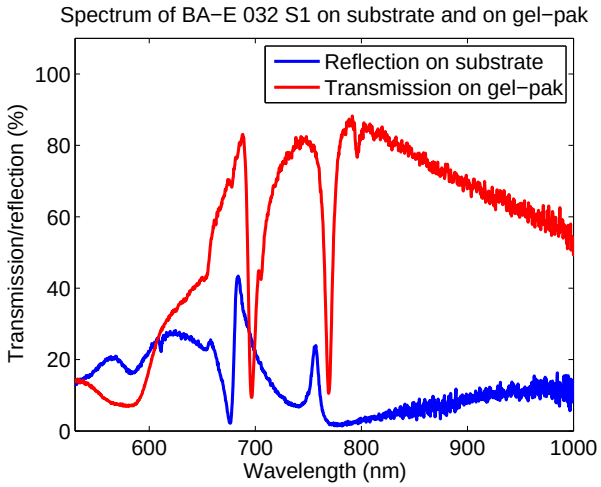

Figure 12: Spectrum of sample BA-E 032, cell S1 on substrate and on gel. The redshift due to the gel, measured by comparing the position of the peaks, is approximately 12.5 nm.

the laser and the polarizer. The light is then sent through a single-mode optical fiber (SMF) and collimated with a $f = 5$ cm lens to a beam of ~ 1 cm diameter. A flip mirror (FM) is used to switch between transmission and reflection measurements; in reflection, a glass plate that is anti-reflection coated on one side is used as a beam splitter (BS) to direct the beam to the aspheric lens L4 ($f = 8$ mm, NA $= 0.5$), which focuses the light onto the photonic-crystal slab. In transmission the light is focused by a similar lens L3 ($f = 8$ mm, NA $= 0.5$). In both cases the light from the membrane is collected by lens L4 and transmitted through the beam splitter. The surface of the photonic-crystal slab is then imaged onto a CCD camera using a $f = 250$ mm lens L5. A second lens could be inserted into the imaging setup, to make a k-space image of the photonic crystal reflection or transmission. The solid and hatched beam paths depicted in figure 13 show the imaging of real-space and k-space respectively.

We used two different CCD camera's, one with a silicon CCD for visible and near-infrared measurements, and one with an InGaAsP CCD for infrared measurements.

4.1 Optical properties

The periodic structure of the membrane causes resonances in the reflection and transmission spectra[1]. Figure 14 shows the measured transmission spectra at normal incidence of the membrane we used (sample BA-E 033, cell B4). This membrane has a lattice constant of 960 nm and an r/a value of ~ 0.28. It has a clear resonance at about 1650 nm, that we ascribe to first order diffraction into the TE waveguide mode.

Using the setup of figure 13 we imaged the reflection and transmission of a strongly focused beam of light from or through the photonic-crystal slab. The result of this for the our pump wavelength and the detection wavelength can be

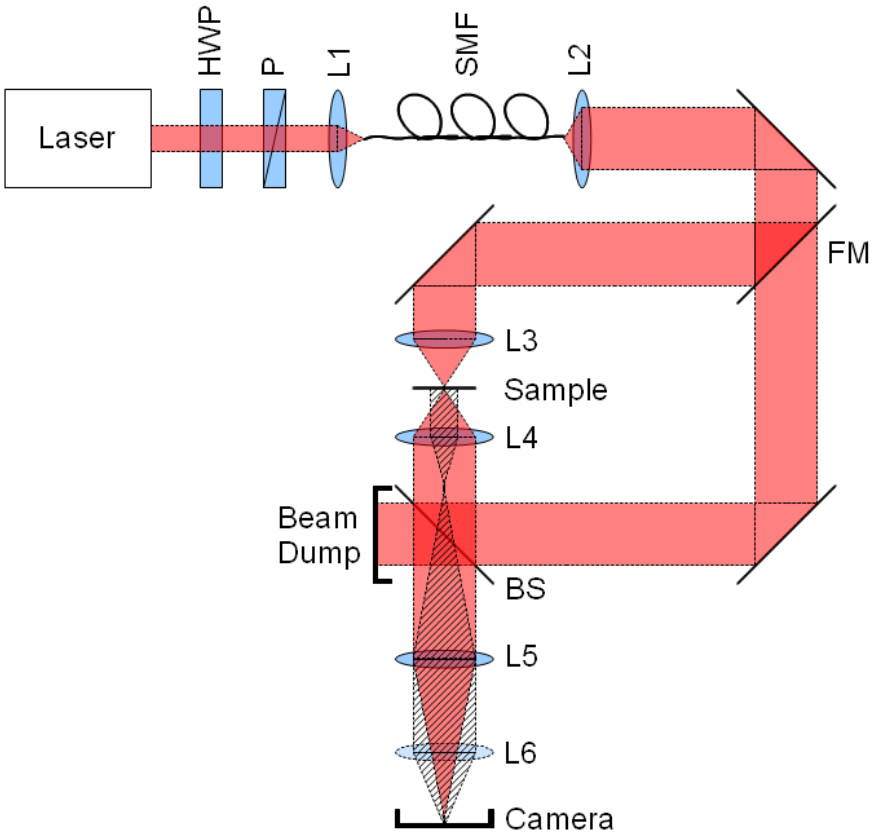

Figure 13: Experimental setup used for imaging of the reflection from and transmission through the photonic-crystal slab. Light from a tunable laser is focused on the sample via either a flip mirror (FM) or a beamsplitter (BS). By inserting the lens L6, the imaging is switched from real-space imaging (solid beam path) to k-space imaging of the reflection or transmission of the photonic-crystal slab (hatched beam path). Details of the setup are found in the text.

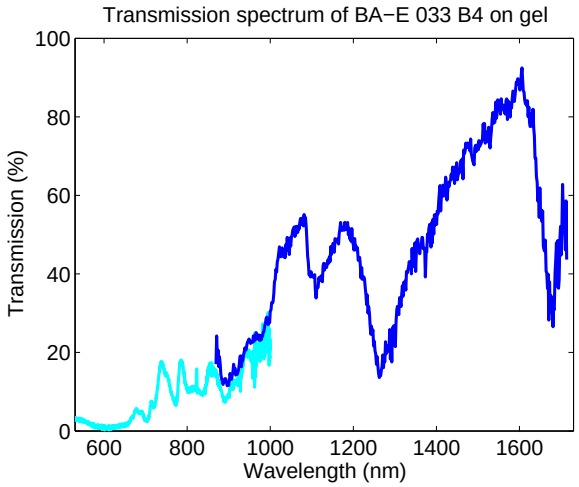

Figure 14: Transmission spectra at normal incidence of sample BA-E 033, cell B4 on the gel.

seen in figure 15.

The images shown are all k-space images, which means the image shows intensity versus the angle with which the light exits the membrane. The edge of the circle represents the maximum angle of 30° for the NA=0.5 lens we used. The images were all made when the membranes were already transferred to the gel.

For the images in figure 15c and 15d, white light from an unpolarized, fiber-coupled Xenon lamp was used to illuminate the sample, and a bandpass filter in front of the camera was used to select only the light with a wavelength of 1550 nm ± 5 nm.

The images in figure 15a and 15b were made using a tunable picosecond Ti:Sapphire laser which was tuned to 775 nm and attenuated to about 5 mW of power using a half-wave plate and a polarizer. The polarization was not controlled or measured, since the polarizer was positioned before a single mode fiber in the setup, which could introduce some depolarization.

From these images we can see that there are clear resonances visible at 1550 nm: in the transmission there is a sharp minimum shaped like a deformed square and a broader minimum as a partly visible dark circle around normal incidence. The edge of the large horizontal and vertical structure is another resonance. At 775 nm, there is also structure visible, but it is a lot harder to identify what exactly the resonances are.

Figure 16 shows a few transmission k-space images where we tuned the imaged wavelength by setting the bandpass filter at an angle to the beam path, still using the Xenon white light source to illuminate the sample. The resonances can easily be seen to shift to different angles at the different wavelengths.

We determine the position of the resonance by measuring the $k_{\|}$ that corresponds to the minimum in transmission (the black circle around normal incidence). The corresponding dispersion of this resonance is shown in figure 17.

The blue dots in figure 17 thus show part of the photonic bandstructure of

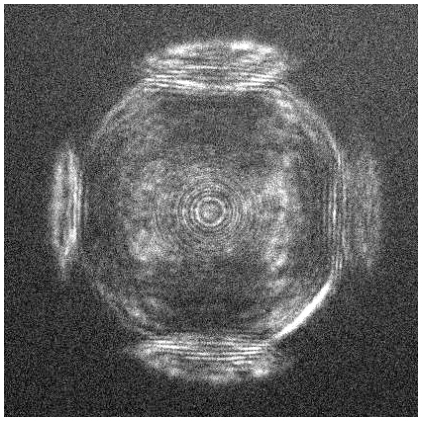

(a) Reflection at 775 nm.

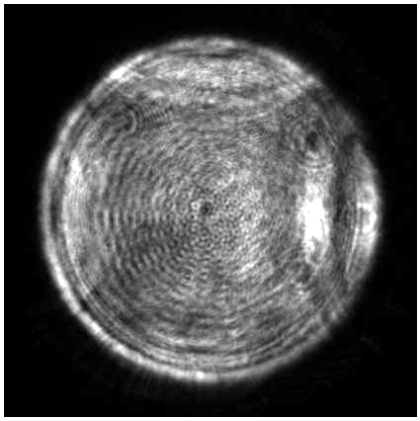

(b) Transmission at 775 nm.

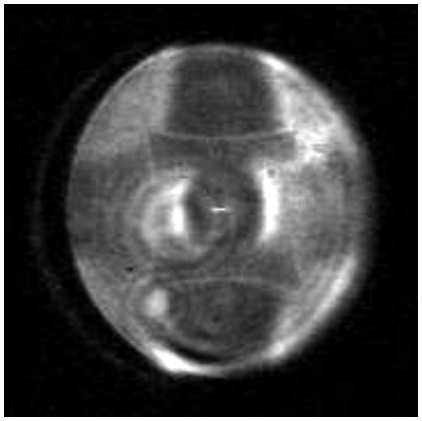

(c) Reflection at 1550 nm.

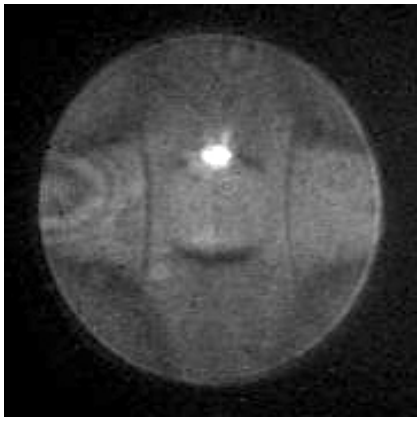

(d) Transmission at 1550 nm.

Figure 15: k-space images of sample BA-E 033, cell B4 at 775 nm and at 1550 nm.

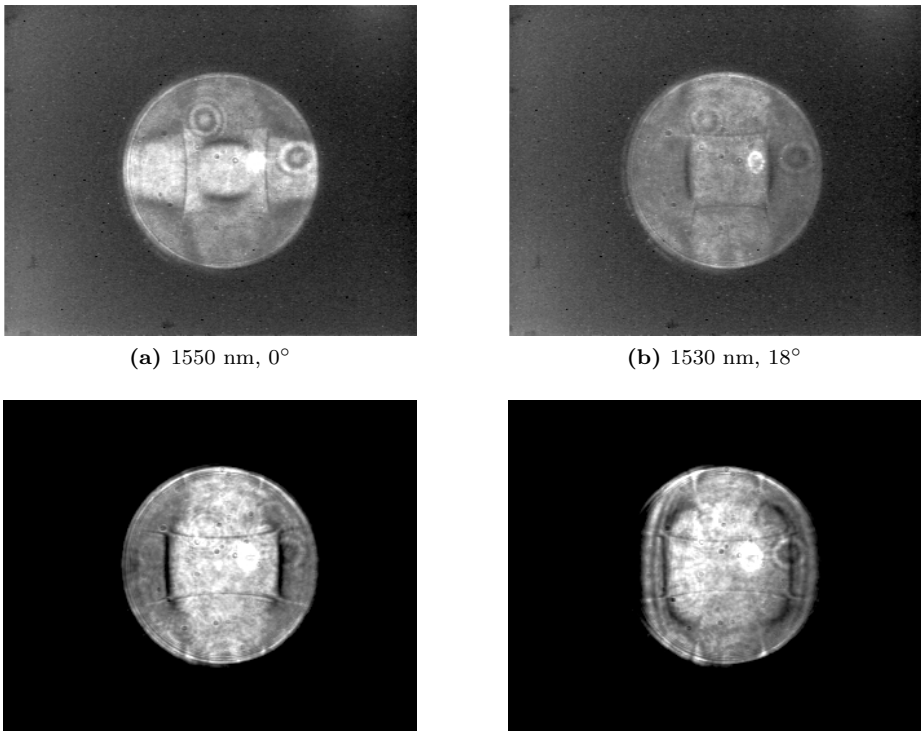

(a) 1550 nm, 0°

(b) 1530 nm, 18°

(c) 1494 nm, 31°

(d) 1482 nm, 34°

Figure 16: k-space images of the transmission of sample BA-E 033, cell B4 for different wavelengths. These images were made using white light and a bandpass filter which was set at an angle with respect to the beam, in order to change it's center frequency.

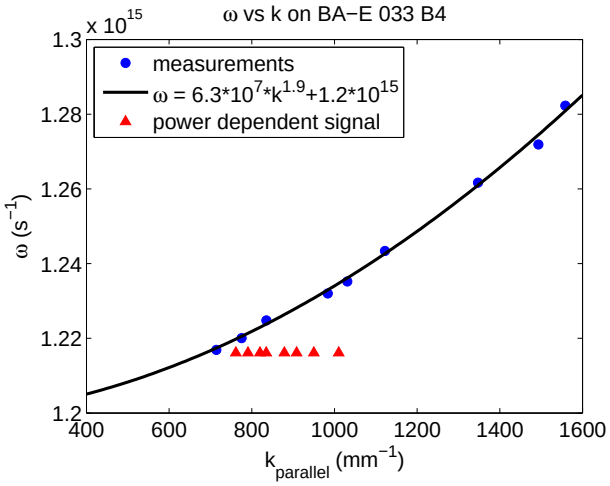

Figure 17: ω vs k on sample BA-E 033, cell B4. The blue dots where obtained by measuring the size of the black 'circle' in the images of figure 16 and calculating $k_{\|}$ from that. The black line is a power law fit of this resonance. The red triangles show the power dependent data of section 4.3, shifted to match the $k_{\|}$ at 0 power to the ω vs k fit.

sample BA-E 033, cell B4. The black line shows the best power law fit ($y = ax^b + c$) to this band. From the fit, it appears this part of the band can be approximated quite well by a quadratic relation. This power law fit also enables us to estimate the frequency of this resonance at normal incidence: at $k_{\|} = 0$ the fit yields $\omega = 1.2 * 10^{15}$ s^{-1}, which corresponds to a wavelength of 1570 nm.

In figure 14 there are no clear resonances visible around 1550–1600 nm. However, the first-order resonance of a square lattice is four-fold degenerate at normal incidence for infinitesimal holes. When the hole size is increased, the bands will split up[4]. A numerical calculation of the band structure for a similar membrane shows that this splitting can be as much as 20 %, and that the 'upper' band (at higher ω, so at lower wavelength) will become very sharp at normal incidence, and thus very hard to detect. This seems to indicate that the resonance which has a minimum at 1680 nm in figure 14 is the 'lower' band and the band in figure 17 is the 'upper' band of the same resonance. The splitting, measured from the position of the minimum in transmission, would be $\sim$ 110 nm, which is about 6.5–7 %.

4.2 Luminescence of the GaAs substrate

Figure 18 shows the measured spectra of luminescence from various positions on sample BA-E 033. To obtain these spectra we focused the pump light on the sample and sent the light from the sample to a grating spectrometer in a normal-incidence reflection setup. The pump was again the Ti:Sapphire laser, tuned to 775 nm. The power on the sample was approximately 200-250 mW, with a spot size of about 100 µm. We used a GaAs substrate as a filter to prevent the pump beam from entering the spectrometer.

We performed this measurement on 3 different positions on the sample:

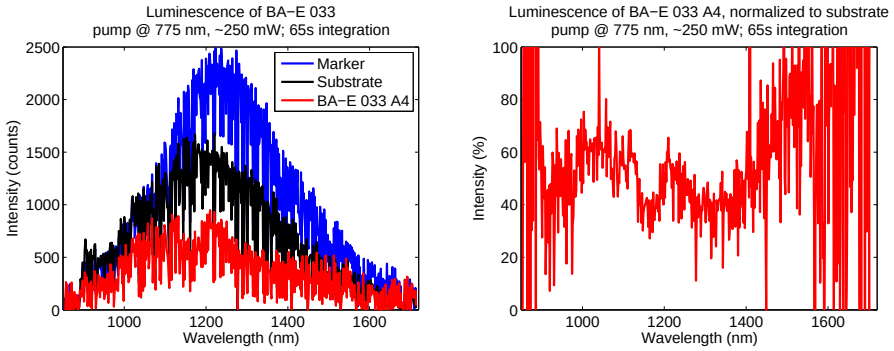

(a) Spectra of the luminescence on the substrate, the marker and on cell A4, all on sample BA-E 033.

(b) Normalized spectrum of the luminescence on sample BA-E 033, cell A4 (normalized to the luminescence at the unpatterned substrate)

Figure 18: Luminescence spectra on sample BA-E 033, pumped with a tunable picosecond Ti:Sapphire laser at 775 nm, with $\sim$ 250 mW on the sample. The integration time of the spectrometer was 65 s.

the unpatterned substrate, one of the membranes and at the 'marker'. At the marker, all of the top layers are etched away, and only the GaAs substrate is illuminated. An AFM measurement confirmed the edge of this marker to be $\sim$ 2 µm, while the top layers are in total only about $\sim$ 1.3 µm thick.

From figure 18a, it can be seen that the measured luminescence was higher on the marker than on the unpatterned substrate. The luminescence at a membrane is lower than on the unpatterned substrate; in figure 18b the luminescence at sample BA-E 033, cell A4 is plotted normalized to the luminescence of the substrate. A dip at around 1150 nm can clearly be seen. The photonic-crystal slab has a resonance at this wavelength (compare figure 14; the reflection spectrum of cell A4 is very similar to that of cell B4 since only the hole size differs slightly).

This means we could be measuring the transmission of the luminescent signal through the photonic-crystal slab. Since the intensity is very low, this is a very inefficient way of measuring the resonances of the photonic-crystal slab.

From the fact that the GaAs substrate at the marker gives a higher signal than outside the marker, where several extra layers are present, we conclude this luminescence occurs largely in the GaAs substrate layer.

4.3 Possible observation of SPDC

Figure 19 shows k-space images at 1550 nm of sample BA-E 033 cell B4, while the membrane was on the gel. The images were made in transmission while illuminating the membrane with the Ti:Sapphire laser, tuned to 775 nm. To ensure only light at 1550 nm is imaged we placed first a piece of GaAs, then a longpass filter for 1400 nm, and then a bandpass filter at 1550 nm with a width of 10 nm in front of the infrared camera.

The structure that is visible in figure 19a resembles the structure at 1550 nm,

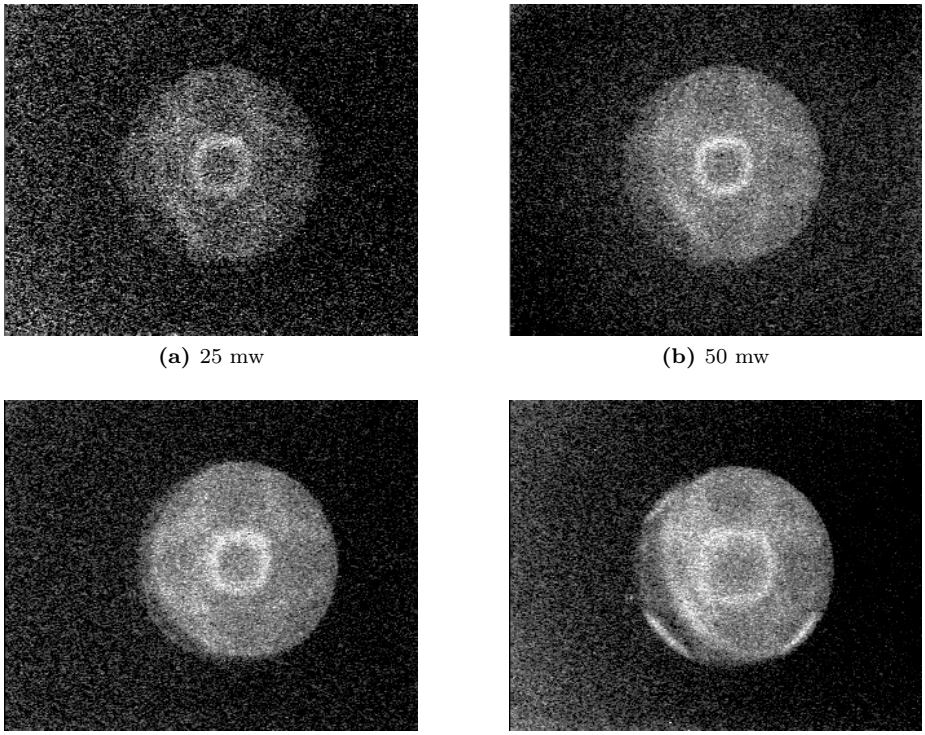

(a) 25 mw **(b)** 50 mw

(c) 75 mw **(d)** 100 mw

Figure 19: k-space images of the signal at 1550 nm. Note how the observed structure changes at high input power. Most notably, the bright ring around normal incidence increases diameter. Brightness and contrast of the images have been changed to enhance the visibility of the structure.

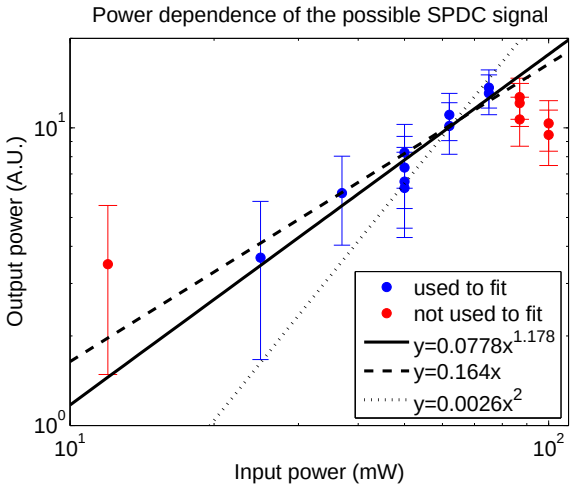

Figure 20: Power dependence of the signal shown in the previous section. The noise in the background is about 3–4 units, as shown by the errorbars. Higher power values are low due to subtracting too much background because of extra light outside of the main spot, while the first data point is about as large as the noise in the background. These values therefore have not been included in the data set to be fitted.

as can be seen in figure 15c and 15d. This confirms that the signal is really at 1550 nm, and not caused by some spurious transmission of the filters at 775 nm.

Another feature which can be observed from these images is that the structure of the resonances changes at high input power. This measurement was reversible, so no permanent damage was done to the membrane — the damage threshold for this sample, when the pump was focused on the membrane, was approximately 10–15 mW, and for the defocused illumination used for these images, about 125–150 mW.

The resonances can be observed to move to larger angles of incidence at higher pump power.

4.4 Power dependence of this signal

In order to gain more insight into the origin of the signal at 1550 nm, we measured its power dependence. For this, we measured k-space images (like the 4 shown in figure 19) for different pump powers. From these images we determined the power of the signal at 1550 nm, by first subtracting a background image, which was measured immediately after each measurement with the laser blocked. We then computed the mean intensity of the pixels outside of the main k-space circle in the resulting image and subtracted that as well. The mean intensity of the k-space circle in the resulting image was then plotted in figure 20.

Where there are multiple data points at the same input power this was actually the same measurement but with different 'dark' images which were taken either directly before or after the actual measurement.

The data is plotted on a logarithmic scale and was fitted with three different models: a power law (solid line), a linear relation (dashed line) and a quadratic relation (dotted line). The first measurement was excluded from the data to fit

because the signal was comparable in size to the noise on the background; the last two measurements were excluded because there was extra light outside of the main spot, which caused a too large substraction of background.

It can be seen in figure 20 that the power law gives the best fit, with a power of 1.18 ± 0.14. This is very close to 1, and thus we can safely exclude any kind of quadratic power dependence.

A quadratic power dependence could have been caused by luminescence that was pumped by two-photon absorption. In that case, two photons are absorbed at the same time, bringing the system in a state with higher energy, which might then cause light to be emitted at higher wavelengths when the system reverts to its earlier state.

4.5 Resonance shifting at high pump power

The wavelength shift of the resonances as a function of pump power can be measured by comparing the structure of the resonances in figure 19 with those in figure 16. Since the structure at 100 mW pump power in 19d resembles the structure at 1530 nm in 16b we can immediately estimate the maximum wavelength shift we measured to be about 20 nm.

We assume the wavelength shift is entirely due to a change in refractive index. In order to plot the change in refractive index as a function of the pump power, we measured the size of the bright circles around normal incidence in the k-space images, of which 4 are shown in figure 19. We then calculated the $k_{\|}$ corresponding to these values.

Because we now measure the maximum instead of the minimum of the resonance, we shift the k-values to correspond to the ones in figure 17, by just taking a linear fit of the $k_{\|}$ as function of power and shifting the $k_{\|}$ at 0 power to the fit line of the ω vs k at 1550 nm. The result can be seen in figure 17 as red triangles.

From the shift in ω, visualized in figure 17 as the vertical distance of the red triangles to the black fit line, we calculated the change in refractive index. We did this by taking the slope of the line from the origin to the measured points, folded back over the zone boundary. The expression for this line is $\omega = c/n(k_{\|} + G)$, where $G = 2\pi/a$ in this case. Thus $\Delta n = -c(k_{\|}+2\pi/a)\Delta\omega/\omega^2$. Here we assumed the change in refractive index is the only contributing factor to the shift of the resonance. The result is shown in figure 21.

Several effects could be involved to cause the wavelength shift. First of all, direct optical creation of free carriers in the material could cause the refractive index to change[12]. However, this would induce a blueshift. We estimate our pump intensity to be comparable to the intensity of [12], and thus estimate a change in refractive index of -0.005 at 1.5 µm. Here we also assume the AlGaAs of the membrane is sufficiently similar to GaAs to justify this.

Thermal effects can also contribute to the shift, via a thermal change in refractive index and via expansion of the lattice. The thermal expansion coefficient of GaAs is 5.7 * 10^{-6} K^{-1}[9], while the refractive index changes with temperature with dn/dT = 2.64 * 10^{-4} K^{-1}[12]. This means that the change in lattice constant due to thermal expansion will be about 2 % of the change in refractive index.

Since, for normal incidence, $\omega = c/n*2\pi/a$, changes in a and n will contribute equally to the change in ω. This means that $d\omega/dT$ due to thermal expansion

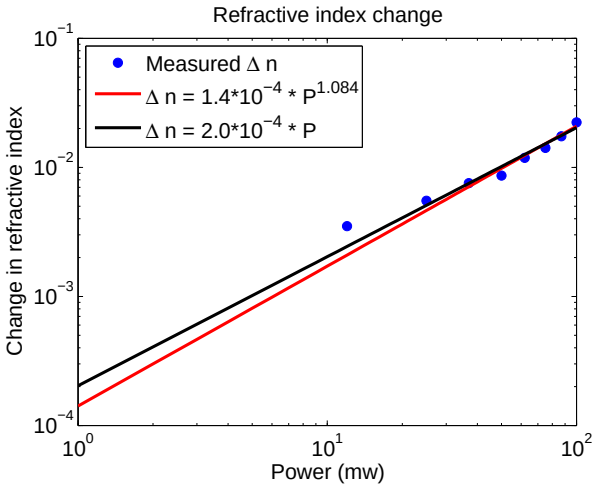

Figure 21: Refractive index change of sample BA-E 033, cell B4 as a function of the pump power. Here the change in lattice constant ($\sim$ 2 % of Δn) is neglected. Also shown are a power-law fit (red line) and a linear fit (black line).

will also be about 2 % of $d\omega/dT$ due to change in refractive index. This justifies that we neglected this contribution before.

In this thermal effect, Δn is proportional to the change in temperature ΔT. If we assume heat conduction is the most important contribution to heat transport away from the membrane, it follows from the fact that heat conduction is a linear function of the temperature difference between the membrane and its environment, that the equilibrium temperature is linear in input power, and Δn is then also linear in input power.

The red and black lines in figure 21 show respectively a power law fit and a linear fit to the refractive index change. The power law fit yields a power of 1.08 ± 0.13, which confirms this linear relation.

From figure 21 we can see the maximum Δn is 0.022. There are 2 contributions to this Δn. The free-carrier contribution is -0.005. This means the thermal contribution is $\Delta n_{thermal} = 0.027$. Now $\Delta T = \Delta n_{thermal}/(dn/dT) =\sim 100$ K. Without considering the free-carrier creation, $\Delta T =\sim 80$ K.

Since the gel retains its integrity up to 220 °C, a temperature difference of up to about 190 K should be possible. Moreover, since the damage threshold was measured to be 125–150 mW, a temperature change of 100 K at 100 mW seems quite probable.

5 Discussion

We observed light at a wavelength of 1550 nm coming from a photonic-crystal slab which was pumped with a laser tuned to 775 nm. The intensity of this signal is very low and is linear in pump power. The two most probable causes for this signal are luminescence and SPDC.

It is very hard to distinguish luminescence and SPDC, since both are basically a source of light, linear in pump power, which is produced in, or coupled to

the modes of the photonic-crystal slab. The detected k-space structure is only determined by the way the light couples out of the membrane, a process that doesn't distinguish how the light was produced.

One way to distinguish between SPDC and luminescence would be to do difference frequency generation by including light at $\lambda_a =\sim 1.5$ µm. The pump beam and the filter before the camera should then be tuned such, that this extra idler beam is not detected, while light with frequency $\omega_b = \omega_p - \omega_a$ is. If SPDC was present, the signal wave at λ_b should be amplified by the incident idle beam at λ_a. If all of the signal was due to luminescence, no such amplification would occur.

6 Summary

We showed Atomic Force Microscopy (AFM) provides a method to measure different properties of the photonic-crystal slabs we use. These include the radius of the holes r, distance between the holes a, r/a and the thickness of various layers. Scanning a larger area with the AFM gives an idea of the height differences that are caused by the buckling of the membrane. Finally, using the AFM to produce force-distance curves provides a method to measure the (local) stiffness of the membrane.

We demonstrated the photonic-crystal slabs can be transferred from their GaAs substrate to a layer of gel, even when the membranes were previously touched down and stuck to the substrate. Since the gel is transparent, this opens the possibility of transmission measurements, and it eliminates the luminescence of the GaAs substrate. The resonances in the photonic bandstructure of the photonic-crystal slabs shift to the red by a few nanometer due to the transfer to the gel.

We showed infrared light with a wavelength of 1550 nm can be observed to be coming from a photonic-crystal slab that is being pumped with a laser tuned to half of this wavelength. The observed band structure and power dependence suggest either SPDC or luminescence as possible origins of this signal. One possible way to distinguish between these two would be to do difference frequency generation in the photonic-crystal slab.

References

[1] V. Astratov *et al.*, "Photonic band-structure effects in the reflectivity of periodically patterned waveguides," *Physical Review B*, vol. 60, pp. 255–258, December 1999.

[2] K. Crozier *et al.*, "Air-bridged photonic crystal slabs at visible and near-infrared wavelengths," *Physical Review B*, vol. 73, March 2006.

[3] J. D. Joannopoulos, S. G. Johnson, J. N. Winn, and R. D. Meade, *Photonic crystals. Molding the flow of light.* Princeton University Press, second ed., 2008.

[4] S. Fan and J. Joannopoulos, "Analysis of guided resonances in photonic crystal slabs," *Physical Review B*, vol. 65, June 2002.

[5] S. Fan, W. Suh, and J. Joannopoulos, "Temporal coupled-mode theory for the fano resonance in optical resonators," *J. Opt. Soc. Am. A*, vol. 20, pp. 569–572, March 2003.

[6] E. Driessen, *Coupling light to periodic nanostructures*. PhD thesis, Leiden University, 2009.

[7] R. W. Boyd, *Nonlinear optics*. Academic Press, second ed., 2003.

[8] F. J. Giessibl, "Advances in atomic force microscopy," *Rev. Mod. Phys.*, vol. 75, pp. 949–983, Jul 2003.

[9] Ioffe Institute, "New semiconductor materials database." `http://www.ioffe.ru/SVA/NSM`.

[10] A. R. Hodges, K. M. Bussmann, and J. H. Hoh, "Improved atomic force microscope cantilever performance by ion beam modification," *Review of Scientific Instruments*, vol. 72, pp. 3880–3883, October 2001.

[11] Gel Pak, "Gel-pak brochure." `http://www.gelpak.com/products/gelpak_brochure.pdf`, 2009.

[12] J. P. Mondia, H. W. Tan, S. Linden, H. M. van Driel, and J. F. Young, "Ultrafast tuning of two-dimensional planar photonic-crystal waveguides via free-carrier injection and the optical kerr effect," *J. Opt. Soc. Am. B*, vol. 22, pp. 2480–2486, November 2005.